

## Exploring vector dark matter via effective interactions

Hrishabh Bharadwaj

*Rajkiya Mahila Mahavidyalaya, Budaun - 243601, Uttar Pradesh, India*  
*Mahatma Jyotiba Phule Rohilkhand University, Bareilly, Uttar Pradesh, India*  
*hrishabhphysics@gmail.com*

Received Day Month Year

Revised Day Month Year

We explore the properties of self-conjugate dark matter (DM) particles that predominantly interact with Standard Model electroweak gauge bosons, using an effective field theory approach. The study emphasizes effective contact interactions, invariant under the Standard Model gauge group, between vector DM and SM-neutral electroweak gauge bosons. Focusing on interaction terms up to dimension-8, we establish constraints on the model parameters based on the observed DM relic density and indirect detection signals. We also examine the prospects for dark matter-nucleon scattering in direct detection experiments. In addition, we analyze the sensitivity of low-energy LEP data to the pair production of light DM particles (with masses up to 80 GeV). Finally, we assess the potential of the proposed International Linear Collider (ILC) to probe these effective operators through the detection of DM particles produced in association with mono-photons.

*Keywords:* Vector dark matter, relic density, Collider, ILC.

PACS numbers:95.35.+d

### 1. Introduction

Dark matter (DM) accounts for approximately 23% of the Universe's energy density and 75% of its total matter, as indicated by various cosmological and astrophysical observations. Precise measurements of DM density from the Planck Collaboration estimate the relic density to be  $\Omega_{DM}h^2 = 0.1198 \pm 0.0012$ .<sup>1</sup> Despite significant advancements in our understanding, the true nature of DM remains unknown.

Efforts to detect DM are underway in multiple areas. Direct detection experiments, such as CRESST,<sup>2</sup> DAMA/LIBRA,<sup>3,4</sup> XENON100,<sup>5,6</sup> CoGeNT,<sup>7</sup> LUX,<sup>8</sup> CDMS,<sup>9</sup> and PandaX-II,<sup>10</sup> aim to observe the recoil of atoms or nucleons as a result of DM interactions. Collider experiments, both current and proposed, focus on detecting DM through mono-jet or di-jet events associated with missing energy. Meanwhile, indirect detection experiments like FermiLAT,<sup>11</sup> HESS,<sup>12</sup> and AMS-02<sup>13,14</sup> search for excess cosmic rays resulting from DM annihilation into Standard Model particles.

The Effective Field Theory (EFT) approach offers a model-independent framework for studying DM-SM interactions by treating them as contact interactions de-

scribed by non-renormalizable operators.<sup>15–23</sup> This formalism enables exploration of DM phenomenology across various processes, including annihilation and scattering. Several studies have constrained the parameter space for DM-quark and DM-gauge boson interactions at the LHC, using simplified models and popular scenarios.<sup>24–28</sup>

In the context of deep inelastic lepton-hadron scattering, analyses of twist-2 operators and their renormalization-group equations have provided insights into DM-nucleon scattering, with contributions from quark operators. Further research into one-loop effects from twist-2 quark and gluonic operators has been conducted, enhancing our understanding of DM-nucleon interactions.<sup>29–32</sup> Collectively, these efforts contribute to ongoing investigations into DM through direct and indirect detection, as well as collider searches.

In this paper, we study DM currents interacting primarily with the Standard Model (SM) electroweak neutral gauge bosons via gauge-invariant effective operators within the  $SU(2)_L \times U(1)_Y$  framework. We consider a real vector dark matter (DM) candidate, focusing on three types of operators, all of which are SM gauge singlets.

In Section 2, we construct the effective interaction Lagrangian for vector DM coupled to SM neutral electroweak gauge bosons, considering higher-dimensional operators. Section 3 presents constraints on the model parameters based on relic density measurements and consistency checks from direct and indirect detection experiments. Section 4 discusses the constraints derived from Large Electron-Positron Collider (LEP) data and assesses the sensitivity of these operators at the proposed International Linear Collider (ILC). Finally, we summarize our findings in Section 5.

## 2. Model

The SM is extended with a set of SM gauge-invariant operators up to dimension 8. The effective Lagrangian describing the interaction between a real vector dark matter particle ( $V$ ) and the SM neutral electroweak gauge bosons is given as follows:

$$\mathcal{L}_V = \frac{\alpha_{S_1}^V}{\Lambda^4} O_{S_1}^V + \frac{\alpha_{S_2}^V}{\Lambda^2} O_{S_2}^V + \frac{\alpha_T^V}{\Lambda^4} O_T^V, \quad (1)$$

where  $\Lambda$  denotes the effective theory's cut-off scale and  $\alpha_i$  is the respective strength of the effective interaction. The effective operators for vector DM are given as:

$$\begin{aligned} O_{S_1}^V &\equiv m_V^2 V^\mu V_\mu B_{\mu\nu} B^{\mu\nu} \\ O_{S_2}^V &\equiv V^\rho V_\sigma B_{\mu\rho} B^{\mu\sigma} \\ O_T^V &\equiv V^\rho i \partial^\mu i \partial^\nu V_\rho \mathcal{O}_{\mu\nu} + \text{h.c.}, \end{aligned} \quad (2)$$

with  $O_{\mu\nu} = B_\mu^\alpha B_{\alpha\nu} - \frac{1}{4} g_{\mu\nu} B^{\alpha\beta} B_{\alpha\beta}$ , where  $B_{\mu\nu}$  represents the field strength tensor associated with the SM  $U(1)_Y$  gauge.

### 3. DM phenomenology

#### 3.1. Relic density

In the early Universe, Dark Matter (DM) particles remained in thermal equilibrium with the plasma through continuous annihilation and production processes. As the Universe expanded and the DM particles became non-relativistic, they gradually deviated from thermal equilibrium. Eventually, they *froze out* and became a cold relic when their annihilation rate dropped below the Hubble expansion rate. This evolution is described by the Boltzmann equation, and the DM relic density can be approximately expressed as follows:<sup>33,34</sup>

$$\Omega_V h^2 \approx 0.12 \sqrt{\frac{g_*(x_f)}{100}} \left(\frac{x_f}{28}\right) \frac{2 \times 10^{-26} \text{ cm}^3/\text{s}}{\langle \sigma v \rangle}, \quad (3)$$

where  $x_f$ ,  $g_*(x_f)$ ,  $\langle \sigma v \rangle$  are the ratio of DM mass and temperature at freeze-out, effective degrees of freedom at freeze-out and thermally averaged DM annihilation cross-section respectively. The thermally averaged cross-section can be written as  $\langle \sigma v \rangle = a + b \langle v^2 \rangle + c \langle v^4 \rangle + \mathcal{O}(v^6)$ , where  $\langle v^2 \rangle = \frac{6}{x_f}$  &  $\langle v^4 \rangle = \frac{60}{x_f^2}$ . The thermally averaged cross-sections for the processes contributing to the dark matter relic density are provided in Appendix A.

We utilized FeynRules<sup>35</sup> to generate the interaction vertices and other necessary model files. These files were then used in the MadDM<sup>36</sup> package to calculate the relic density. Figure 1 shows contour plots in the  $\Lambda - m_V$  plane, where the current DM relic density of  $\Omega h^2 = 0.1198^1$  is satisfied for DM masses ranging from 10 GeV to 1 TeV. The areas below the contour lines are consistent with the relic density constraints. In all relic density calculations, the coupling strengths  $\alpha_i$  were set to 1.

#### 3.2. Indirect detection

The annihilation of dark matter in dense regions of the Universe would produce a significant amount of high-energy SM particles. The High Energy Stereoscopic System (H.E.S.S.)<sup>37</sup> employs indirect detection methods to search for DM by observing high-energy gamma rays from specific regions, such as the galactic center or dwarf galaxies. H.E.S.S. aims to identify possible signals resulting from DM annihilation or decay, which can generate gamma rays as secondary particles when DM interacts and converts into SM particles. By accurately measuring gamma-ray fluxes and energy spectra, H.E.S.S. provides valuable insights into the properties and distribution of DM, helping to place constraints on its parameters.

The expressions for the cross-section of DM annihilation into a photon pair are given below:

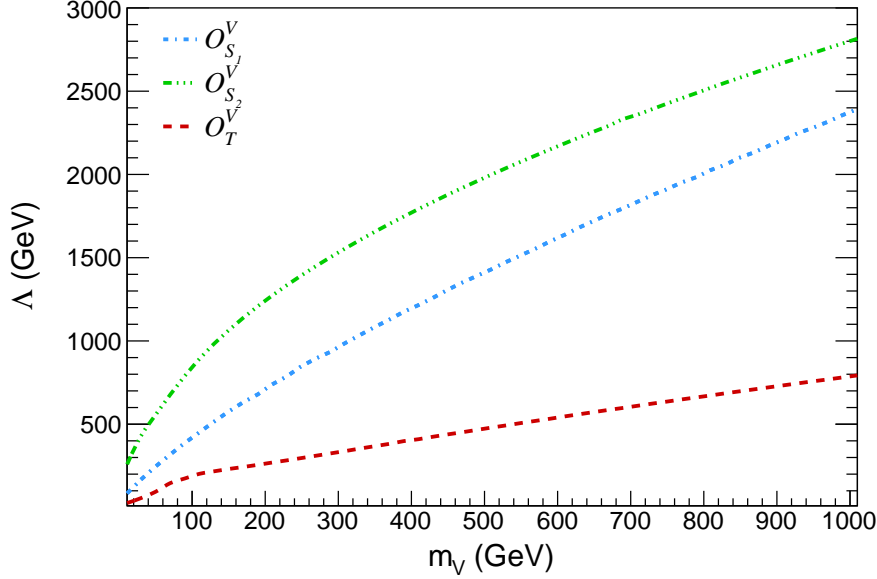


Fig. 1: The contour lines correspond to DM relic density  $\Omega h^2 = 0.1198$  for respective DM operators. The parameter space below the contour line is allowed from the relic density observations.

$$\sigma_{S_1}^V v (V V \rightarrow \gamma\gamma) \simeq \frac{16 \alpha_{S_1}^{V^2}}{\pi} \cos^4 \theta_w \frac{m_V^6}{\Lambda^8} \left( 7 + \frac{5}{3} v^2 \right) \quad (4)$$

$$\sigma_{S_2}^V v (V V \rightarrow \gamma\gamma) \simeq \frac{\alpha_{S_2}^{V^2}}{\pi} \cos^4 \theta_w \frac{m_V^2}{\Lambda^4} \left( 7 + \frac{5}{3} v^2 \right) \quad (5)$$

$$\sigma_T^V v (V V \rightarrow \gamma\gamma) \simeq \frac{2 \alpha_T^{V^2}}{\pi} \cos^4 \theta_w \frac{m_V^6}{\Lambda^8} \left( 1 + \frac{5}{3} v^2 \right) \quad (6)$$

We investigate dark matter (DM) masses ranging from 10 GeV to 1 TeV. In the indirect detection cross-sections provided in equations (4)-(6), the terms independent of the DM relative velocity  $v$  arise purely from s-wave annihilation, while the terms proportional to  $v^2$  correspond to p-wave annihilation. We assume a DM relative velocity of approximately  $10^{-3} c$ . The equations in (4)-(6) indicate that all relevant operators exhibit s-wave behavior. When calculating the DM annihilation cross-section into photon pairs, we use parameters consistent with relic density constraints for the given DM mass  $m_V$ . For each  $m_V$ , the corresponding annihilation cross-section  $\sigma v$  is shown in Fig. 2. The region above each line is allowed, while the shaded area represents the exclusion zone from H.E.S.S. indirect detection limits.

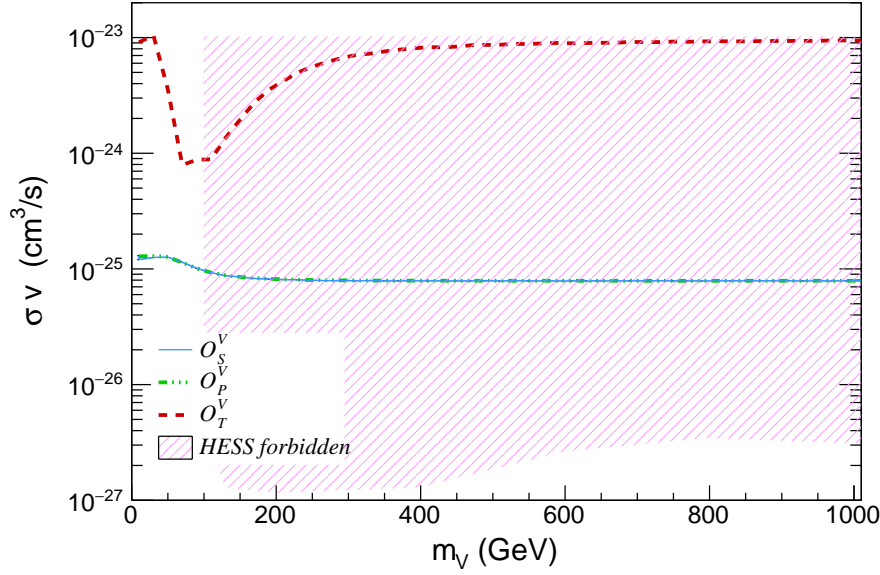


Fig. 2: Variation of the DM annihilation cross-section into  $\gamma\gamma$  for each operator, depicted by colored lines, as a function of the DM mass, while keeping all other parameters consistent with the observed relic density. The shaded region is excluded based on data from H.E.S.S.

### 3.3. DM-nucleon interaction

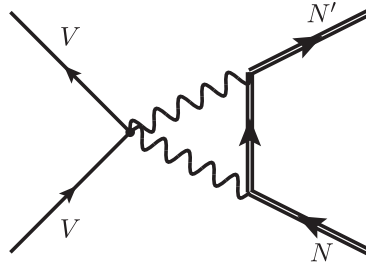


Fig. 3: Feynman diagram depicting the scattering of dark matter particles with nucleons.

Experiments targeting direct detection<sup>2-10</sup> aim to observe the scattering of dark matter (DM) particles with nucleons or atoms. These experiments are specifically designed to measure the recoil momentum of nucleons or atoms within the detector material. Scattering events are generally classified into three categories: (i) DM-

nucleon, (ii) DM-atom, and (iii) DM-electron interactions. In our model, where DM does not directly interact with leptons, quarks, or gluons at the tree level, such interactions can only occur at loop levels. This is illustrated for DM-nucleon scattering in Figure 3, which represents the next area of focus in our ongoing research.

#### 4. Collider searches

##### 4.1. Constraints from LEP

By utilizing existing findings and observations from LEP data, we can establish constraints on effective operators. The cross-section for the process  $e^+e^- \rightarrow \gamma^* + VV$  is compared with the combined analysis conducted by the DELPHI and L3 collaborations for  $e^+e^- \rightarrow \gamma^* + Z \rightarrow q\bar{q} + \nu_l\bar{\nu}_l$  at a center-of-mass energy  $\sqrt{s} = 196.9$  GeV, with an integrated luminosity of  $0.679 \text{ fb}^{-1}$ . Here,  $q$  represents the light quarks  $u$ ,  $d$ , and  $s$ , while  $\nu_l$  denotes the Standard Model neutrinos, including  $\nu_e$ ,  $\nu_\mu$ , and  $\nu_\tau$ .

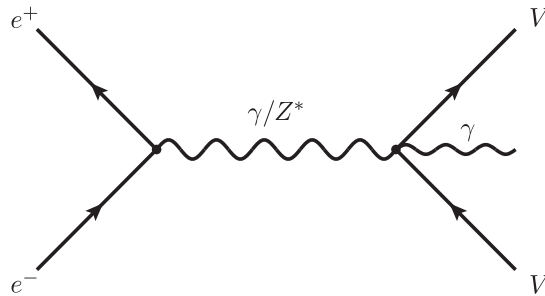


Fig. 4: Feynman diagram for the production of a dark matter pair with a photon in an  $e^+e^-$  collider.

The Feynman diagrams contributing to the production of a photon  $\gamma$  with missing energy, arising from effective operators as described in equation (2), at the  $e^-, e^+$  lepton collider are shown in Figure 4. The measured cross-section for this process is found to be  $0.055 \text{ pb}$ , with a statistical error  $\Delta\sigma_{\text{stat.}}$ , a systematic error  $\Delta\sigma_{\text{sys.}}$ , and a total error  $\Delta\sigma_{\text{total}}$  of  $0.031 \text{ pb}$ ,  $0.008 \text{ pb}$ , and  $0.032 \text{ pb}$ , respectively, as reported in.<sup>38</sup> Therefore, the contribution from an additional channel involving final states with dark matter pairs, resulting in missing energy and two quark jets, can be constrained based on the observed  $\Delta\sigma_{\text{total}}$ . In Figure 5, we present dashed line contours at a 95% confidence level that correspond to  $\Delta\sigma_{\text{total}} \simeq 0.032 \text{ pb}$ , related to the operators in the DM mass- $\Lambda$  plane. The region below the dashed lines, as indicated, is excluded by the combined analysis of LEP, while the solid lines represent the relic density contours.

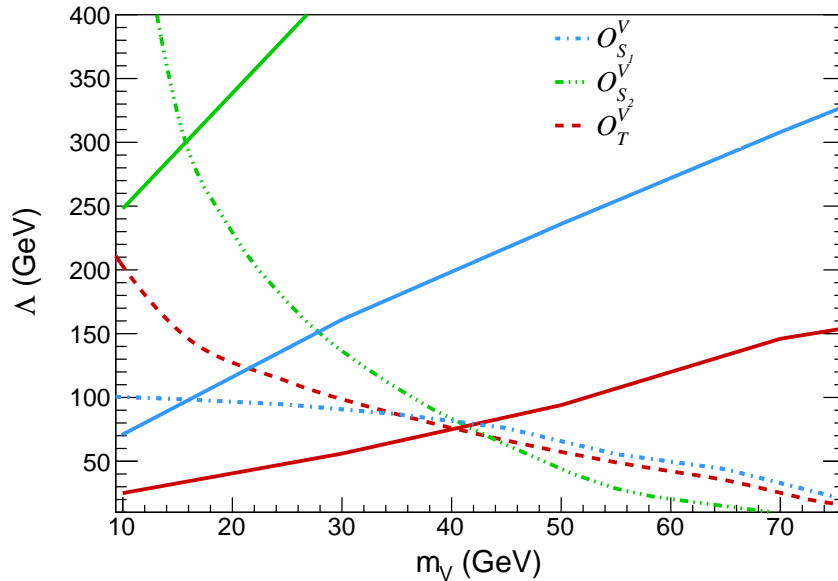


Fig. 5: Dashed lines illustrate the contours within the parameter space defined by the DM mass and the kinematic reach for (a)  $e^+e^- \rightarrow V V + \gamma^* \rightarrow \cancel{E}_T + q_i \bar{q}_i$  at a center-of-mass energy of  $\sqrt{s} = 196.9$  GeV, considering an integrated luminosity of  $679.4 \text{ pb}^{-1}$ . These contours adhere to the constraint  $\delta\sigma_{\text{tot}} = 0.032 \text{ pb}$ , derived from the combined analysis of DELPHI and L3.<sup>38</sup> The region below the dashed lines is excluded based on LEP observations. Additionally, the regions below the solid lines corresponding to specific operators satisfy the relic density constraint  $\Omega_{\text{DM}} h^2 \leq 0.1198$ .

#### 4.2. Constraints from ILC

We now examine the processes involving DM pair production along with mono-photon at the proposed International Linear Collider (ILC) for a DM mass spectrum ranging from approximately 10 to 250 GeV. The specific process we consider is  $e^+e^- \rightarrow V V \gamma$ , as illustrated in Figure 4. The primary Standard Model background for the  $e^+e^- \rightarrow \cancel{E}_T \gamma$  process originates from  $e^+e^- \rightarrow Z \gamma \rightarrow \nu \bar{\nu} \gamma$ .

The examination of background and signal processes, utilizing the accelerator parameters outlined in the technical design report for the ILC<sup>39,40</sup> and presented in Table 1, involves the simulation of SM background and DM signals. Model files are generated using FeynRules,<sup>35</sup> and events are produced with MadGraph.<sup>41</sup> For event selection and analysis, MadAnalysis 5<sup>42</sup> has been employed.

In addition to the basic selection criteria, which include cuts on the transverse momentum of the photon ( $p_{T_\gamma} \geq 10 \text{ GeV}$ ) and the pseudo-rapidity of the photon

	<i>ILC-250</i>	<i>ILC-500</i>
$\sqrt{s}$ (GeV)	250	500
$L_{int}$ ( $fb^{-1}$ )	250	00
$\sigma_{BG}$ (pb)	1.07	1.48

Table 1: Accelerator parameters

( $|\eta_\gamma| \leq 2.5$ ), a selection requirement pertaining to the photon energy in the context of on-shell production is applied. Specifically, events are excluded if the following condition is met:

$$\frac{2E_\gamma}{\sqrt{s}} = 1 - \frac{(m_Z^2 \pm 10 m_Z \Gamma_Z)}{s} \quad (7)$$

This means that events are rejected when  $2E_\gamma/\sqrt{s}$  falls within the intervals  $[0.8, 0.9]$  and  $[0.95, 0.98]$  for center-of-mass energies ( $\sqrt{s}$ ) of 250 GeV and 500 GeV, respectively.

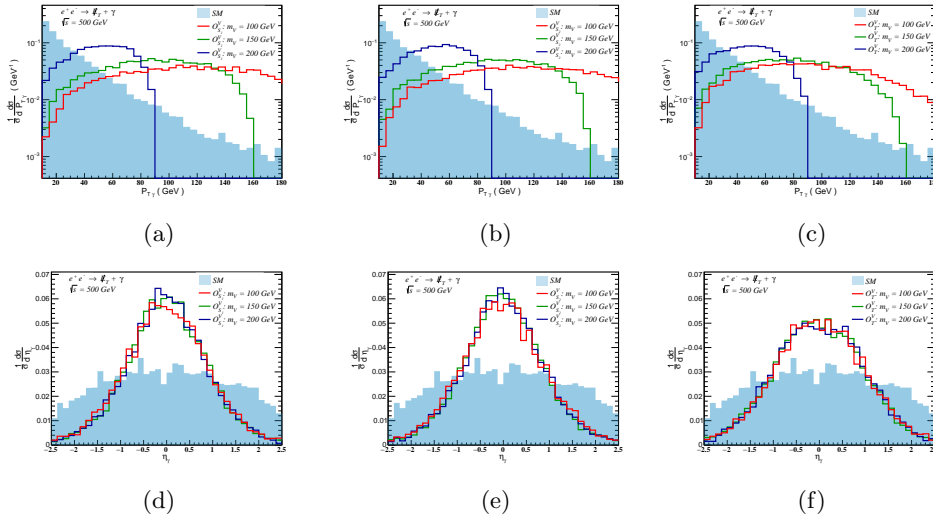


Fig. 6: Normalized one-dimensional differential cross-sections relative to  $p_{T\gamma}$  (upper panel) and  $\eta_\gamma$  (lower panel) for both Standard Model processes and those influenced by the  $O_{S_1}^V$ ,  $O_{S_2}^V$ , and  $O_T^V$  operators, presented at three selected dark matter masses: 100, 150, and 200 GeV.

Because of their high sensitivity, we focus on the kinematic observables  $p_{T\gamma}$  and  $\eta_\gamma$  when analyzing the form profiles of processes involving mono-photons with

missing energy. We produce normalized one-dimensional distributions for the signals created by important operators as well as the background processes of the Standard Model. We present the normalized differential cross-sections in figures 6a - 6f for three different DM mass values, 100, 150, and 200 GeV, taking into account a center-of-mass energy of  $\sqrt{s} = 500$  GeV and an integrated luminosity of  $500 \text{ fb}^{-1}$  in order to investigate the effect of DM mass.

The calculation of  $\chi^2$  utilizing the double differential distributions of kinematic observables,  $p_{T,\gamma}$  and  $\eta_\gamma$ , increases the sensitivity of  $\Lambda$  to the dark matter mass. Under the following circumstances, this analysis is carried out for both background and signal processes:

- (i) Considering an integrated luminosity of  $250 \text{ fb}^{-1}$ , with a DM mass range of 10 GeV to 125 GeV at a center-of-mass energy ( $\sqrt{s}$ ) of 250 GeV.
- (ii) Considering an integrated luminosity of  $500 \text{ fb}^{-1}$ , with a DM mass range of 10 GeV to 250 GeV at a center-of-mass energy ( $\sqrt{s}$ ) of 500 GeV.

The  $\chi^2$  is defined as

$$\chi^2 = \sum_{i=1}^{n_1} \sum_{j=1}^{n_2} \left[ \frac{N_{ij}^{NP}}{\sqrt{N_{ij}^{SM+NP} + \delta_{\text{sys}}^2 (N_{ij}^{SM+NP})^2}} \right]^2. \quad (8)$$

In this case, the new physics and total differential events inside the two-dimensional grid of  $p_{T,\gamma_i}$  and  $\eta_{\gamma_j}$  are represented by  $N_{ij}^{NP}$  and  $N_{ij}^{SM+NP}$ , respectively. The measurement's overall systematic error is denoted by the notation  $\delta_{\text{sys}}$ .

To compute the  $\chi^2$ , we run simulations for two-dimensional differential distributions using the collider parameters listed in Table 1 and a cautious estimate of a 1% systematic error. We provide  $3\sigma$  contours in the  $m_{DM} - \Lambda$  plane at the 99.73% confidence level in Figs. 7a to 7b. For effective operators that follow perturbative unitarity, these contours correspond to center-of-mass energies of  $\sqrt{s} = 250$  GeV and 500 GeV, respectively.

## 5. Summary

The phenomenology of dark matter is examined in this article using an effective field theory as a framework. Neutral electroweak gauge bosons and DM particles are studied in the context of SM gauge-invariant contact interactions up to dimension 8. The study is restricted to self-conjugate DM particles, namely a real vector boson, in order to preserve the invariance of SM gauge symmetry above the electroweak scale. The observed relic density of  $\Omega_{DM} h^2 = 0.1198 \pm 0.0012$  is used to evaluate the relic density contributions of these particles and constrain their characteristics. Furthermore, the operators for the DM mass  $> 100$  GeV are severely constrained by comparing the annihilation cross-sections for the specified DM mass with indirect detection data from H.E.S.S.

The phenomenologically interesting DM mass range of  $\leq 30$  GeV for  $O_{S_1}^V$ ,  $\leq 20$  GeV for  $O_{S_2}^V$ , and  $\leq 22 = 5$  GeV for  $O_T^V$  operators, respectively, is disallowed,

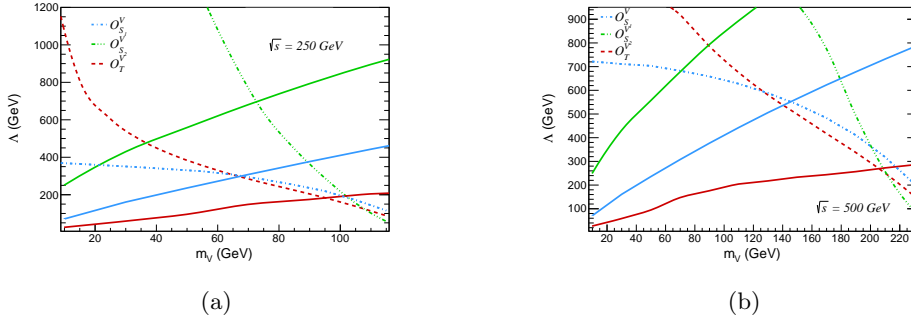


Fig. 7: Dashed lines present  $3\sigma$  contours with 99.73% confidence level in the  $m_{\text{DM}} - \Lambda_{\text{eff}}$  plane, derived from  $\chi^2$  analyses of the  $e^+e^- \rightarrow \cancel{E}_T + \gamma$  signature at the proposed International Linear Collider (ILC) designed for  $\sqrt{s} = 250$  GeV, with an integrated luminosity of  $250 \text{ fb}^{-1}$ . The region below each dashed line, corresponding to its respective contour, is potentially discoverable with a confidence level of at least 99.73%. Additionally, the regions below the solid lines corresponding to specific operators satisfy the relic density constraint  $\Omega_{\text{DM}} h^2 \leq 0.1198$ .

according to the analysis, which is extended to existing LEP data. For the pair generation of DM particles at the proposed ILC, a  $\chi^2$ -analysis is then carried out, encompassing a DM mass range of around  $10 - 250$  GeV for the operators discussed in the section 2. The results show that the dominating mono-photon signal at the proposed electron-positron collider, ILC, can provide greater sensitivity within the  $m_V - \Lambda$  parameter space that is constrained by relic density and indirect detection data.

### Appendix A.

The expressions for thermally averaged cross-section for DM annihilation to photon pair production are calculated to be:

$$\langle \sigma_{S_1}^V v \rangle (V V \rightarrow \gamma\gamma) \simeq \frac{16 \alpha_{S_1}^{V^2}}{\pi} \cos^4 \theta_w \frac{m_V^6}{\Lambda^8} \left( 7 + \frac{10}{x_f} \right) \quad (\text{A.1})$$

$$\langle \sigma_{S_2}^V v \rangle (V V \rightarrow \gamma\gamma) \simeq \frac{\alpha_{S_2}^{V^2}}{\pi} \cos^4 \theta_w \frac{m_V^2}{\Lambda^4} \left( 7 + \frac{10}{x_f} \right) \quad (\text{A.2})$$

$$\langle \sigma_T^V v \rangle (V V \rightarrow \gamma\gamma) \simeq \frac{2 \alpha_T^{V^2}}{\pi} \cos^4 \theta_w \frac{m_V^6}{\Lambda^8} \left( 1 + \frac{10}{x_f} \right) \quad (\text{A.3})$$

The expressions for thermally averaged cross-section for DM annihilation to  $Z$

pair production are calculated to be:

$$\begin{aligned} \langle \sigma_{S_1}^V v \rangle (V V \rightarrow ZZ) &\simeq \frac{\alpha_{S_1}^{V^2}}{\pi} \sin^4 \theta_w \frac{m_V^6}{\Lambda^8} \\ &\times \left[ 136 - 128 \frac{m_V^2}{m_Z^2} + 96 \frac{m_V^4}{m_Z^4} - 80 \frac{m_Z^2}{m_V^2} + 24 \frac{m_Z^4}{m_V^4} + \frac{1}{x_f} \left( 384 - 752 \frac{m_V^2}{m_Z^2} + 608 \frac{m_V^4}{m_Z^4} + 16 \frac{m_Z^2}{m_V^2} - 64 \frac{m_Z^4}{m_V^4} \right) \right] \end{aligned} \quad (\text{A.4})$$

$$\begin{aligned} \langle \sigma_{S_2}^V v \rangle (V V \rightarrow ZZ) &\simeq \frac{\alpha_{S_2}^{V^2}}{\pi} \sin^4 \theta_w \frac{m_V^2}{\Lambda^4} \\ &\times \left[ \frac{17}{2} - 8 \frac{m_V^2}{m_Z^2} + 6 \frac{m_V^4}{m_Z^4} - 5 \frac{m_Z^2}{m_V^2} + \frac{3}{2} \frac{m_Z^4}{m_V^4} + \frac{1}{x_f} \left( 24 - 47 \frac{m_V^2}{m_Z^2} + 38 \frac{m_V^4}{m_Z^4} + \frac{m_Z^2}{m_V^2} - 4 \frac{m_Z^4}{m_V^4} \right) \right] \end{aligned} \quad (\text{A.5})$$

$$\begin{aligned} \langle \sigma_T^V v \rangle (V V \rightarrow ZZ) &\simeq \frac{\alpha_T^{V^2}}{\pi} \sin^4 \theta_w \frac{m_V^6}{\Lambda^8} \\ &\times \left[ \frac{11}{2} - 2 \frac{m_V^2}{m_Z^2} + 2 \frac{m_V^4}{m_Z^4} - 4 \frac{m_Z^2}{m_V^2} + 3 \frac{m_Z^4}{m_V^4} + \frac{1}{x_f} \left( 37 - 29 \frac{m_V^2}{m_Z^2} + 26 \frac{m_V^4}{m_Z^4} - \frac{29}{2} \frac{m_Z^2}{m_V^2} + 3 \frac{m_Z^4}{m_V^4} \right) \right] \end{aligned} \quad (\text{A.6})$$

The expressions for thermally averaged cross-section for DM annihilation to  $Z \gamma$  production are calculated to be:

$$\begin{aligned} \langle \sigma_{S_1}^V v \rangle (V V \rightarrow Z\gamma) &\simeq \frac{\alpha_{S_1}^{V^2}}{\pi} \cos^2 \theta_w \sin^2 \theta_w \frac{m_V^6}{\Lambda^8} \\ &\times \left[ 80 + 16 \frac{m_V^2}{m_Z^2} - \frac{63}{2} \frac{m_Z^2}{m_V^2} + 2 \frac{m_Z^4}{m_V^4} + \frac{1}{x_f} \left( 123 + 60 \frac{m_V^2}{m_Z^2} - \frac{31}{4} \frac{m_Z^2}{m_V^2} - \frac{13}{4} \frac{m_Z^4}{m_V^4} \right) \right] \end{aligned} \quad (\text{A.7})$$

$$\begin{aligned} \langle \sigma_{S_2}^V v \rangle (V V \rightarrow Z\gamma) &\simeq \frac{\alpha_{S_2}^{V^2}}{\pi} \cos^2 \theta_w \sin^2 \theta_w \frac{m_V^2}{\Lambda^4} \\ &\times \left[ 5 + \frac{m_V^2}{m_Z^2} - \frac{63}{32} \frac{m_Z^2}{m_V^2} + \frac{1}{8} \frac{m_Z^4}{m_V^4} + \frac{1}{x_f} \left( \frac{123}{16} + \frac{15}{4} \frac{m_V^2}{m_Z^2} - \frac{31}{64} \frac{m_Z^2}{m_V^2} - \frac{13}{64} \frac{m_Z^4}{m_V^4} \right) \right] \end{aligned} \quad (\text{A.8})$$

$$\begin{aligned} \langle \sigma_T^V v \rangle (V V \rightarrow Z\gamma) &\simeq \frac{\alpha_T^{V^2}}{\pi} \cos^2 \theta_w \sin^2 \theta_w \frac{m_V^6}{\Lambda^8} \\ &\times \left[ \frac{51}{8} + \frac{3}{2} \frac{m_Z^2}{m_V^2} + \frac{3}{32} \frac{m_Z^4}{m_V^4} + \frac{1}{x_f} \left( \frac{153}{4} - \frac{45}{8} \frac{m_Z^2}{m_V^2} + \frac{9}{32} \frac{m_Z^4}{m_V^4} \right) \right] \end{aligned} \quad (\text{A.9})$$

## References

1. N. Aghanim *et al.* [Planck], *Astron. Astrophys.* **641** (2020), A6 [erratum: *Astron. Astrophys.* **652** (2021), C4] doi:10.1051/0004-6361/201833910 [arXiv:1807.06209 [astro-ph.CO]].
2. G. Angloher *et al.* [CRESST], *Eur. Phys. J. C* **77** (2017) no.5, 299 doi:10.1140/epjc/s10052-017-4878-6 [arXiv:1612.07662 [hep-ex]].

3. R. Bernabei, P. Belli, F. Cappella, V. Caracciolo, S. Castellano, R. Cerulli, C. J. Dai, A. d'Angelo, S. d'Angelo and A. Di Marco, *et al.* Eur. Phys. J. C **73** (2013), 2648 doi:10.1140/epjc/s10052-013-2648-7 [arXiv:1308.5109 [astro-ph.GA]].
4. R. Bernabei, P. Belli, A. Bussolotti, F. Cappella, V. Caracciolo, R. Cerulli, C. J. Dai, A. d'Angelo, A. Di Marco and H. L. He, *et al.* Universe **4** (2018) no.11, 116 doi:10.3390/universe4110116
5. E. Aprile *et al.* [XENON100], Phys. Rev. D **94** (2016) no.12, 122001 doi:10.1103/PhysRevD.94.122001 [arXiv:1609.06154 [astro-ph.CO]].
6. E. Aprile *et al.* [XENON], Eur. Phys. J. C **77** (2017) no.12, 881 doi:10.1140/epjc/s10052-017-5326-3 [arXiv:1708.07051 [astro-ph.IM]].
7. C. E. Aalseth *et al.* [CoGeNT], Phys. Rev. D **88** (2013), 012002 doi:10.1103/PhysRevD.88.012002 [arXiv:1208.5737 [astro-ph.CO]].
8. D. S. Akerib *et al.* [LUX], Phys. Rev. Lett. **118** (2017) no.2, 021303 doi:10.1103/PhysRevLett.118.021303 [arXiv:1608.07648 [astro-ph.CO]].
9. R. Agnese *et al.* [CDMS], Phys. Rev. Lett. **111** (2013) no.25, 251301 doi:10.1103/PhysRevLett.111.251301 [arXiv:1304.4279 [hep-ex]].
10. X. Cui *et al.* [PandaX-II], Phys. Rev. Lett. **119** (2017) no.18, 181302 doi:10.1103/PhysRevLett.119.181302 [arXiv:1708.06917 [astro-ph.CO]].
11. M. Ackermann *et al.* [Fermi-LAT], Phys. Rev. Lett. **115** (2015) no.23, 231301 doi:10.1103/PhysRevLett.115.231301 [arXiv:1503.02641 [astro-ph.HE]].
12. A. Abramowski *et al.* [H.E.S.S.], Phys. Rev. Lett. **110** (2013), 041301 doi:10.1103/PhysRevLett.110.041301 [arXiv:1301.1173 [astro-ph.HE]].
13. M. Aguilar *et al.* [AMS], Phys. Rev. Lett. **113** (2014), 121102 doi:10.1103/PhysRevLett.113.121102
14. M. Aguilar *et al.* [AMS], Phys. Rev. Lett. **117** (2016) no.9, 091103 doi:10.1103/PhysRevLett.117.091103
15. J. Y. Chen, E. W. Kolb and L. T. Wang, Phys. Dark Univ. **2** (2013), 200-218 doi:10.1016/j.dark.2013.11.002 [arXiv:1305.0021 [hep-ph]].
16. Y. J. Chae and M. Perelstein, JHEP **05** (2013), 138 doi:10.1007/JHEP05(2013)138 [arXiv:1211.4008 [hep-ph]].
17. A. Rajaraman, T. M. P. Tait and A. M. Wijangco, Phys. Dark Univ. **2** (2013), 17-21 doi:10.1016/j.dark.2012.12.001 [arXiv:1211.7061 [hep-ph]].
18. Y. Farzan and A. R. Akbarieh, JCAP **10** (2012), 026 doi:10.1088/1475-7516/2012/10/026 [arXiv:1207.4272 [hep-ph]].
19. G. Arcadi, A. Djouadi and M. Kado, Phys. Lett. B **805** (2020), 135427 doi:10.1016/j.physletb.2020.135427 [arXiv:2001.10750 [hep-ph]].
20. G. Krnjaic and T. Trickle, Phys. Rev. D **108** (2023) no.1, 015024 doi:10.1103/PhysRevD.108.015024 [arXiv:2303.11344 [hep-ph]].
21. T. Nomura and X. Xu, [arXiv:2405.17885 [hep-ph]].
22. H. Bharadwaj and A. Goyal, Chin. Phys. C **45** (2021) no.2, 023114 doi:10.1088/1674-1137/abce50 [arXiv:2008.13621 [hep-ph]].
23. E. Singh, H. Bharadwaj and Devisharan, Int. J. Mod. Phys. A **39** (2024) no.11n12, 2450038 doi:10.1142/S0217751X24500386 [arXiv:2406.14389 [hep-ph]].
24. R. C. Cotta, J. L. Hewett, M. P. Le and T. G. Rizzo, Phys. Rev. D **88** (2013), 116009 doi:10.1103/PhysRevD.88.116009 [arXiv:1210.0525 [hep-ph]].
25. A. Crivellin, U. Haisch and A. Hibbs, Phys. Rev. D **91** (2015), 074028 doi:10.1103/PhysRevD.91.074028 [arXiv:1501.00907 [hep-ph]].
26. N. Chen, J. Wang and X. P. Wang, [arXiv:1501.04486 [hep-ph]].

27. N. F. Bell, J. B. Dent, A. J. Galea, T. D. Jacques, L. M. Krauss and T. J. Weiler, *Phys. Rev. D* **86** (2012), 096011 doi:10.1103/PhysRevD.86.096011 [arXiv:1209.0231 [hep-ph]].
28. H. Bharadwaj, S. Dutta and A. Goyal, *JHEP* **11** (2021), 056 doi:10.1007/JHEP11(2021)056 [arXiv:2109.02586 [hep-ph]].
29. M. Drees and M. Nojiri, *Phys. Rev. D* **48** (1993), 3483-3501 doi:10.1103/PhysRevD.48.3483 [arXiv:hep-ph/9307208 [hep-ph]].
30. J. Hisano, K. Ishiwata and N. Nagata, *Phys. Rev. D* **82** (2010), 115007 doi:10.1103/PhysRevD.82.115007 [arXiv:1007.2601 [hep-ph]].
31. J. Hisano, K. Ishiwata, N. Nagata and M. Yamanaka, *Prog. Theor. Phys.* **126** (2011), 435-456 doi:10.1143/PTP.126.435 [arXiv:1012.5455 [hep-ph]].
32. J. Hisano, doi:10.1093/oso/9780198855743.003.0011 [arXiv:1712.02947 [hep-ph]].
33. M. Bauer and T. Plehn, *Lect. Notes Phys.* **959** (2019), pp. Springer, 2019, doi:10.1007/978-3-030-16234-4 [arXiv:1705.01987 [hep-ph]].
34. S. Dodelson, Academic Press, 2003, ISBN 978-0-12-219141-1
35. A. Alloul, N. D. Christensen, C. Degrande, C. Duhr and B. Fuks, *Comput. Phys. Commun.* **185** (2014), 2250-2300 doi:10.1016/j.cpc.2014.04.012 [arXiv:1310.1921 [hep-ph]].
36. F. Ambroggi, C. Arina, M. Backovic, J. Heisig, F. Maltoni, L. Mantani, O. Mattelaer and G. Mohlabeng, *Phys. Dark Univ.* **24** (2019), 100249 doi:10.1016/j.dark.2018.11.009 [arXiv:1804.00044 [hep-ph]].
37. H. Abdalla *et al.* [H.E.S.S.], doi:10.5281/zenodo.1421098 [arXiv:1810.04516 [astro-ph.HE]].
38. S. Schael *et al.* [ALEPH, DELPHI, L3, OPAL and LEP Electroweak], *Phys. Rept.* **532** (2013), 119-244 doi:10.1016/j.physrep.2013.07.004 [arXiv:1302.3415 [hep-ex]].
39. T. Behnke, J. E. Brau, P. N. Burrows, J. Fuster, M. Peskin, M. Stanitzki, Y. Sugimoto, S. Yamada, H. Yamamoto and H. Abramowicz, *et al.* [arXiv:1306.6329 [physics.ins-det]].
40. T. Behnke, J. E. Brau, B. Foster, J. Fuster, M. Harrison, J. M. Paterson, M. Peskin, M. Stanitzki, N. Walker and H. Yamamoto, [arXiv:1306.6327 [physics.acc-ph]].
41. J. Alwall, R. Frederix, S. Frixione, V. Hirschi, F. Maltoni, O. Mattelaer, H. S. Shao, T. Stelzer, P. Torrielli and M. Zaro, *JHEP* **07** (2014), 079 doi:10.1007/JHEP07(2014)079 [arXiv:1405.0301 [hep-ph]].
42. E. Conte, B. Fuks and G. Serret, *Comput. Phys. Commun.* **184** (2013), 222-256 doi:10.1016/j.cpc.2012.09.009 [arXiv:1206.1599 [hep-ph]].